# Photoelectrochemical determination of alkaline phosphatase activity based on a photo-excited electron transfer strategy

Jiuying Tian, Yanting Yang, Mingjuan Huang, Chunhong Zhou, Jusheng Lu


www.elsevier.com/locate/talanta

PII: S0039-9140(18)31355-9
DOI: https://doi.org/10.1016/j.talanta.2018.12.079
Reference: TAL19427

To appear in: *Talanta*

Received date: 22 October 2018
Revised date: 12 December 2018
Accepted date: 25 December 2018

Cite this article as: Jiuying Tian, Yanting Yang, Mingjuan Huang, Chunhong Zhou and Jusheng Lu, Photoelectrochemical determination of alkaline phosphatase activity based on a photo-excited electron transfer strategy, *Talanta,* https://doi.org/10.1016/j.talanta.2018.12.079

# Photoelectrochemical determination of alkaline phosphatase activity based on a photo-excited electron transfer strategy

Jiuying Tian, Yanting Yang, Mingjuan Huang, Chunhong Zhou, Jusheng Lu*

*Jiangsu Key Laboratory of Green Synthetic Chemistry for Functional Materials, School of Chemistry and Materials Science, Jiangsu Normal University, Xuzhou 221116, PR China*

*Corresponding author at: School of Chemistry and Materials Science, Jiangsu Normal University, 101 Shanghai Road, Xuzhou 221116, PR China. Tel.: +86-516-83403165. jushenglu@jsnu.edu.cn (J. Lu)



## Abstract

A sensitive photoelectrochemical (PEC) biosensor for determination of alkaline phosphatase (ALP) activity was constructed based on a photo-excited electron transfer strategy. Immobilization of CdTe quantum dots (QDs) on $TiO_2$ nanotube arrays (TNAs), addition of iron (III) and adenosine triphosphate (ATP) in turn can effectively adjust the photocurrent response of TNAs under visible light irradiation due to a photo-excited electron transfer process, and alkaline phosphatase (ALP) activity can be determined for its catalysis toward dephosphorylation of ATP. The preparation of CdTe QDs, construction of TNA/QD PEC biosensor and the mechanism of photo-excited electron transfer are investigated in the present work. Under the optimal experimental conditions, the TNA/QD PEC biosensor shows a low limits of detection (LODs)

(0.05 U $L^{-1}$) and limits of quantification detection (LOQs) (0.15 U $L^{-1}$), wide linear range from 0.2 to 15 U $L^{-1}$, and good selectivity towards ALP determination, which has been successfully applied for human serum analysis with good precision (RSD ≤ 5.4%) and high accuracy (recovery rate, 91% -112%).

**Keywords:** Photoelectrochemical; Alkaline phosphatase; $TiO_2$ nanotube arrays; Photo-excited electron transfer

## 1. Introduction

As a common enzyme in human body, alkaline phosphatase (ALP) could catalyze the hydrolysis or transphosphorylation of various phosphoric acid monoesters, including biological macromolecules and small organic molecules in alkaline medium [1,2]. The normal concentration of ALP in adult serum is 20-160 U $L^{-1}$ [3], and some diseases, such as diabetes, liver dysfunction, bone disease and prostate cancer, could cause abnormally elevated ALP levels [4-6]. Therefore, construction of a sensitive analytical method for ALP activity is important for the clinical diagnosis of ALP-related diseases. To date, some analytical methods have been developed for determination of ALP activity, including colorimetric [7-9], electrochemical [4,10,11], fluorescence [12-14], and photoelectrochemical (PEC) analysis [15,16]. In which, the PEC assay exhibits an excellent analytical performance due to the separation of excitation signal from detection signal [17-19]. For example, Chen and co-workers developed a nanochannels PEC biosensor for the detection of ALP activity based on the biocatalytic precipitation controlled photoresponses of the cathodic photocurrents [15]. Shen et al. developed a simple double-channel

PEC sensor for ALP activity based on differential signal between the measuring and reference PEC cells [16]. However, to the best of our knowledge, there has no report of PEC analysis for ALP determination based on an electron transfer mechanism.

$TiO_2$ nanotube arrays (TNAs) have a large surface area and one-dimensional nanostructure with tubular symmetry like other porous nanomaterials [20-23], and have been used in PEC biosensing due to the good biocompatibility and photochemical stability [24]. However, TNAs can only be excited by ultraviolet light due to the wide band gap [25,26], limiting their direct PEC application. In recent years, many attempts have been made to photosensitize $TiO_2$ for visible light response [27-32]. In the present works, to sensitively determine ALP activity, we first prepared TNAs on titanium foil substrate by the electrochemical anodization according to our previously reported method [33]. Then the CdTe QDs were immobilized on the TNAs by covalent bond to form a TNA/QD biosensor, which could improve the visible light response of TNAs. Due to the electrostatic interaction of CdTe QDs and iron (III), a photo-excited electron transfer (PET) process would occur, where CdTe QDs acted as a donor and iron (III) as an electron acceptor [34], leading to the photocurrent decrease of TNA/QD. Addition of adenosine triphosphate (ATP) and ALP in turn would make the photocurrent of TNA/QD recovery and decrease again because of the chelation reaction between iron (III) and ATP and the catalysis of ALP toward ATP. Based on this mechanism, a sensitive PEC biosensor for determination of ALP activity would be constructed, and the specific construction process was shown in Scheme 1.

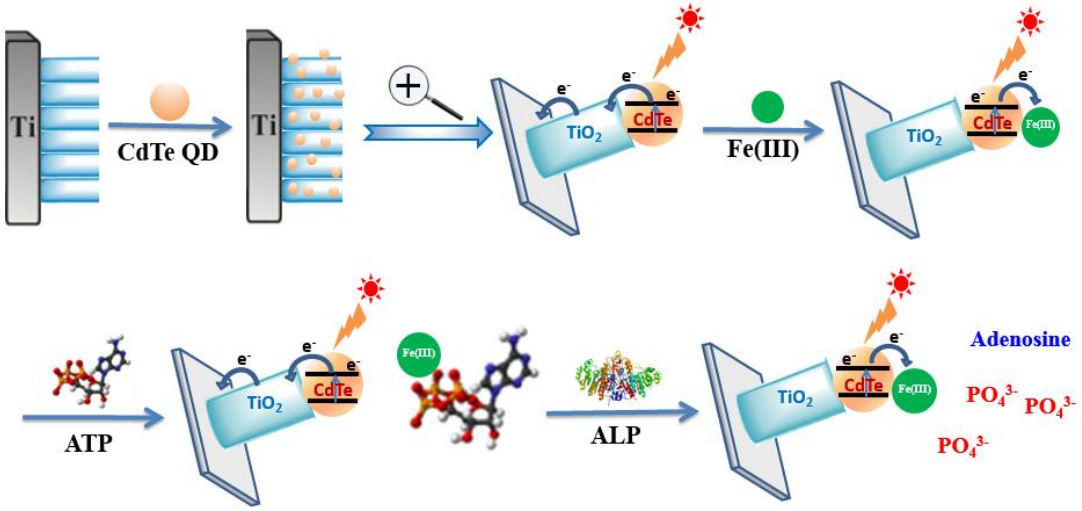


**Scheme 1.** Construction process of the TNA/QD biosensor for determination of ALP activity based on a photo-excited electron transfer strategy.

## 2. Experimental

### *2.1. Materials and reagents*

Titanium foils, tellurium powder, sodium borohydride, cadmium chloride hemi (pentahydrate), L-cysteine, ATP and ALP from bovine intestinal mucosa (EC 3.1.3.1, 670 U $mL^{-1}$) were purchased from Sigma-Aldrich Co., Ltd. (St. Louis, MO, USA). Glycerol and $NH_4F$ were obtained from Sinopharm Chemical Reagent Co., Ltd. (Shanghai, China). All chemicals and materials were used as received unless otherwise noted. Deionized water (18.2 MΩ cm) was prepared from a Milli-Q water purification system and used in the present work.

### *2.2. Apparatus*

The morphology of all nanomaterials was characterized by Hitachi S-4800 scanning electron microscope (Japan) and JEM-2100 transmission electron microscope (JEOL, Japan, acceleration voltage of 200kV), respectively. X-ray photoelectron spectroscopy (XPS) was conducted on a Thermo ESCALAB 250XI instrument with Al Kα X-ray source. UV-vis absorption spectra and fluorescence spectra were drawn by UV-2450 spectrometer (Shimadzu, Japan) and F-4600 FL

spectrophotometer (Hitachi, Japan), respectively. PEC measurements were carried out on a CHI660E electrochemical workstation (CH Instruments, Austin, USA) with a conventional three-electrode system, in which, a TNA/QD was used as the working electrode, a saturated calomel electrode (SCE) was used as the reference electrode and a platinum wire electrode was used as the counter electrode, respectively.

*2.3. Preparation of CdTe QDs capped with L-cysteine*

NaHTe solution was prepared by mixing $NaHB_4$ (1 mmol) and Te powder (0.4 mmol) in 10 mL of $N_2$ saturated water at 80 $^oC$ for 30 min. Then, 2.0 mmol of $CdCl_2$ and 4.0 mmol of L-cysteine were mixed in a 50 mL of $N_2$ saturated solution, and adjusted the pH to about 10.0. Under stirring, 2.0 mL of freshly prepared NaHTe solution was added through a syringe into the above solution at room temperature (RT) with the molar ratio of Cd: L-cysteine: Te of 1: 2: 0.4, and refluxed at 100 $^oC$ under $N_2$ flow for 30 min to produce the CdTe QDs. Ethanol was added to precipitate CdTe QDs, which was centrifuged and washed with ultrapure water for several times. Then the purified CdTe QDs were dispersed in ultrapure water and stored in a dark environment for subsequent use.

*2.4. Construction of TNA/QD PEC biosensor and determination of ALP activity*

For construction of the TNA/QD PEC biosensor, the Ti/TNA was immersed in 100.0 μL of dried dimethyl sulfoxide (DMSO) containing 100 μg of N, N'-carbonyldiimidazole (CDI) at 4 $^oC$ for 2 h in the dark, then immersed in a 200-μL solution of the above-prepared CdTe QDs and incubated for 1 h with slight stirring. Finally, the TNA/QD was washed with water for several times and stored at 4 $^oC$ for the following use. Prior to determination of ALP activity. 0.4 μM of iron (III) and 0.5 μM of ATP was mixed in 200 μL of 10 mM Tris-HCl buffer solution (pH 8.0),

shaken thoroughly and equilibrated for 30 min before PEC measurements, immersed the TNA/QD and measured the photocurrent under visible light irradiation, which was $I_0$, then added ALP with different concentration into the above system and kept at RT for 20 min, determined the photocurrent value, which was *I*. Therefore, the ALP activity could be determined by the photocurrent change value of the TNA/QD PEC biosensor ($\Delta I=I_0-I$). To investigate the inhibition efficiency of $Na_3VO_4$ toward ALP, 5.0 μL of $Na_3VO_4$ solution with different concentration was initially added into 5.0 μL of 1.0 mU ALP solution for 20 min, then added into the PEC system similar to the determination procedure of ALP activity.

## 3. Results and discussion

*3.1. Construction and characterization of TNA/QD PEC biosensor*

To construct a TNA/QD PEC biosensor, CdTe QDs were firstly synthesized and capped with L-cysteine to ensure the stability. The results showed that, with the increase of preparation time, the fluorescence emission wavelength of QDs increased from 532 to 560 nm (Fig. 1A), which displayed different colors from green to yellow under UV light irradiation (inset of Fig. 1A). At the same time, the absorption peaks of CdTe QDs were red-shifted from 485 to 530 nm and all in the visible light region (Fig. 1B), indicating that the electron transfer from the valence band (VB) to the conduction band (CB) of CdTe QDs would be easy to occur under visible light irradiation. However, CdTe QDs prepared for a long time were not stable. When the preparation time was 90 min, CdTe QDs had relatively high fluorescence intensity and stability, and had an average size of 3.5 nm as seen from the TEM image (Fig. 1C). In addition, the as-prepared CdTe QDs capped with l-cysteine could be verified by FT-IR spectra (Fig. 1D). For free L-cysteine (curve a of Fig. 1D), the peaks of 1586 $cm^{-1}$ and 1393 $cm^{-1}$ were corresponded to the carboxyl group, the

absorption peaks at 3176 $cm^{-1}$ and 2077 $cm^{-1}$ indicated the existence of the $–NH_3^+$ group of free L-cysteine. The peak at around 3400 $cm^{-1}$ indicated the $-NH_2$ group, while the peak at 2550 $cm^{-1}$ represented the thiol group. Compared to free L-cysteine, only the characteristic peaks of the carboxyl and amino groups were observed on the L-cysteine-CdTe QDs (curve b of Fig. 1D). It was because that, the covalent affinity of $Cd^{2+}$ to the S-H group of L-cysteine resulted in the disappearance of the thiol group vibration on the L-cysteine-CdTe QDs, which proved the covalent combination of CdTe QDs and L-cysteine.

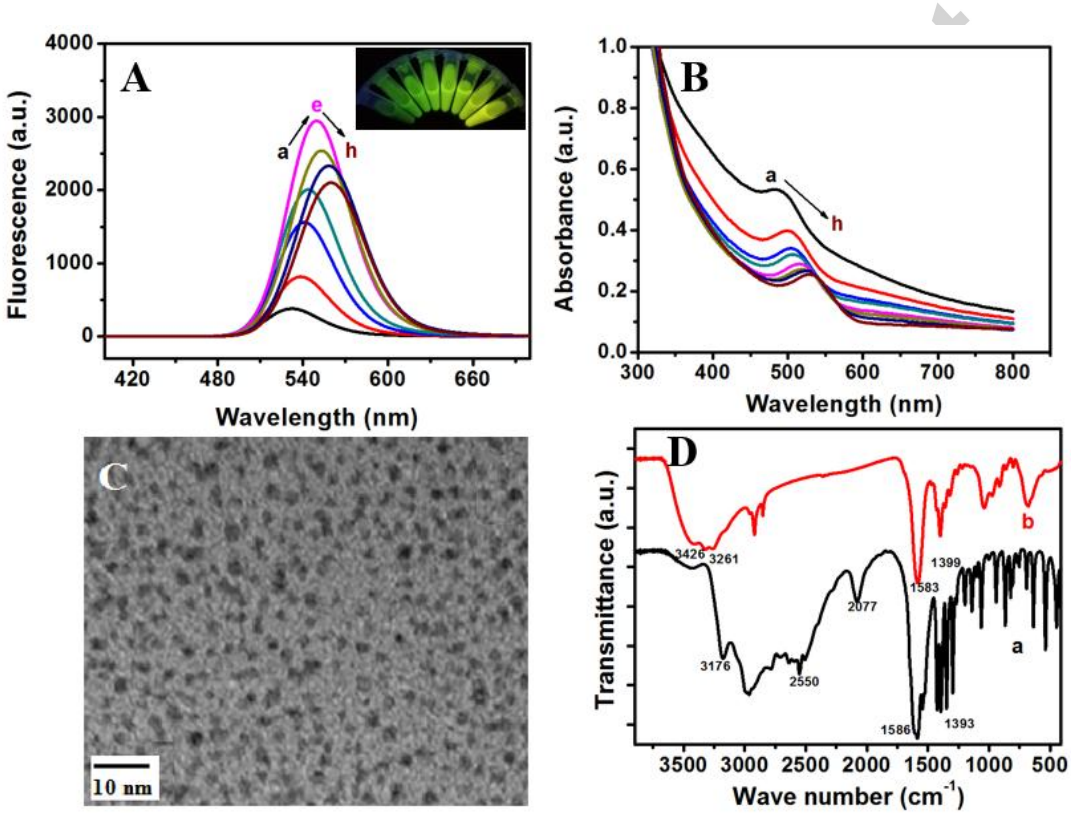


**Fig. 1.** Fluorescence emission spectra (A) and UV-vis absorption spectra (B) of CdTe QDs for various reaction times (a-h: 10 min, 20 min, 30 min, 60 min, 90 min, 120 min, 150 min and 210 min. λex = 360 nm). Inset: the photograph of L-cysteine-CdTe QDs prepared for various time under 365 nm UV light irradiation. (C) TEM image of CdTe QDs. (D) FT-IR spectra of the free L-cysteine (a) and L-cysteine-CdTe QDs (b).

As shown in Fig. 2 A and B, the TNAs fabricated by electrochemical anodization technique with a potential of 20 V for 4h had an average length of 3.0 μm and the inner diameter of ~ 100

nm, which were arranged with a typical ordered porous structure in continuous arrays, and could offer a large interior and outer surface area [35-37]. After immersing the activated TNA in CdTe QD solution for 1 h, CdTe QDs were clearly observed on the TNAs from the SEM image (Fig. 2C), and the EDX showed the existence of Cd, Te, Ti and O (Fig. 2 D to H). In addition, the XPS survey spectrum of TNA/QD and corresponding high resolution XPS spectra of Ti 2p, O 1s, Cd 3d and Te 3d were shown in Fig. 2 I-M, in which, the peaks at 459.2 and 465.0 eV for Ti 2p3/2 and Ti 2p1/2 indicated a $Ti^{4+}$ state in $TiO_2$ (Fig. 2J), two divided peaks at 530.8 and 532.5 eV in the O 1s spectra (Fig. 2K) were attributed to the crystal lattice oxygen of Ti-O in $TiO_2$ and surface hydroxyl groups, respectively. The peaks at 405.8 and 412.1 eV (Fig. 2L) were ascribed to the Cd 3d5/2 and Cd 3d3/2 states of $Cd^{2+}$ in CdTe, respectively. Furthermore, the two peaks in Fig. 2M were attributed to the Te 3d5/2 at 572.5 eV and Te 3d3/2 at 582.8 eV of $Te^{2-}$. All of these suggested the successful construction of the TNA/QD PEC biosensor.

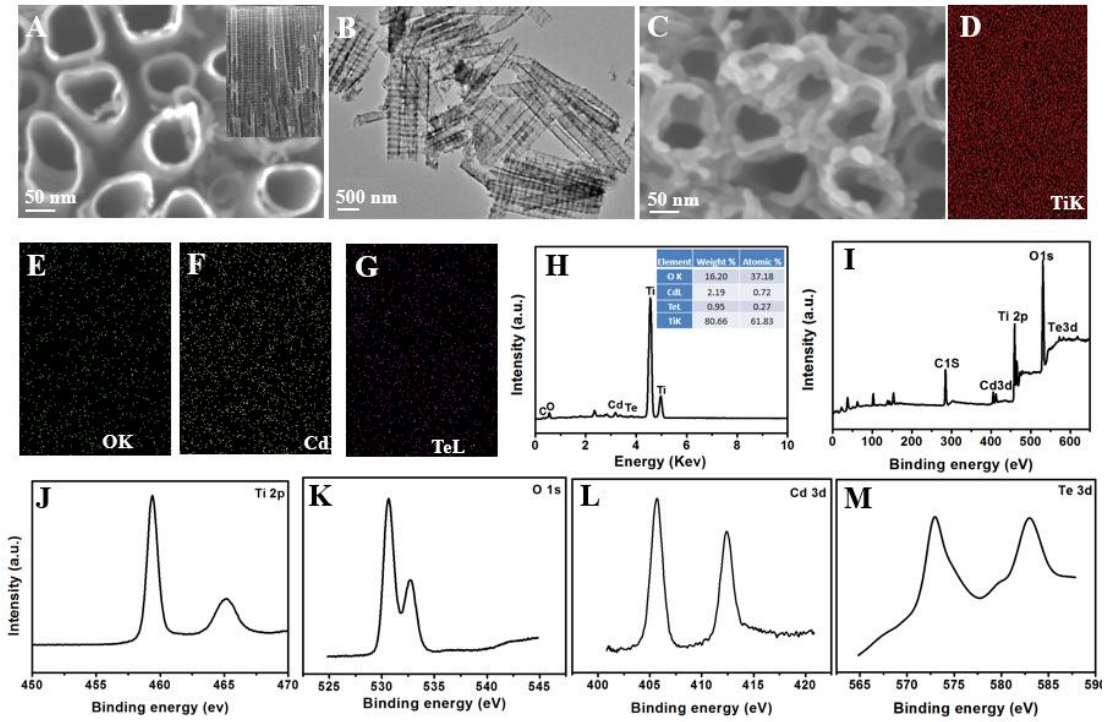


**Fig. 2.** (A) SEM top-view and cross section images (Inset) of TNAs. (B) TEM images of TNAs. (C) SEM top-view image of TNA/QD. (D-H) Energy dispersive X-ray spectroscopy (EDX) of TNA/QD and corresponding

element distribution mapping of Cd, Te, Ti and O. XPS survey spectrum of TNA/QD (I) and high-resolution XPS spectra of Ti 2p (J), O 1s (K), Cd 3d (L) and Te 3d (M).

*3.2. Fluorescent property of CdTe QDs and mechanism of TNA/QD biosensor for determination of ALP activity*

When iron (III) ion was added in the CdTe QDs solution, the fluorescence intensity of CdTe QDs decreased gradually with the increase of iron (III) concentration (Fig. 3A), which indicated that the formation of iron (III)-CdTe complex efficiently induced the photo-excited electron transfer from CdTe QDs to iron (III) ion, leading to the fluorescence quenching. Further addition ATP into iron (III)-CdTe solution, the fluorescence intensity recovered (Fig. 3B), reflecting that ATP seized iron (III) ion from iron (III)-CdTe, and CdTe QDs were in a free state, leading to the fluorescence recovery, which provided the feasibility for subsequent determination of ALP activity with PEC technique.

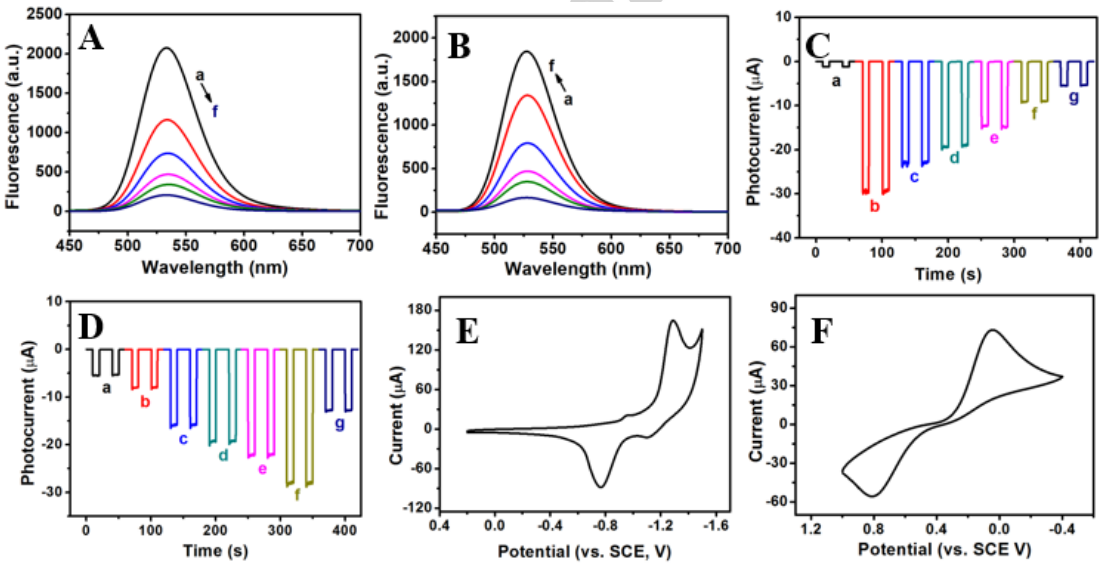


**Fig. 3.** Fluorescence change of CdTe QDs after addition of iron (III) with different concentration (a-f: 0-0.4 μM) (A), then added ATP with different concentration (a-f: 0-0.5 μM) (B), λex = 360 nm. (C) Photocurrent response of TNA (a), TNA/QD (b) and TNA/QD after addition of iron (III) with different concentration (c-g: 0-0.4 μM), (D) Photocurrent response of TNA/QD in 0.4 μM of iron (III) solution containing ATP with different concentration (a-f:

0-0.5 μM), applied potential, +0.2 V. (E) Cyclic voltammogram of TNA/QD, (F) Cyclic voltammogram of iron (III), electrolyte solution: 0.1 M NaCl, scan rate: 0.1 V $s^{-1}$.

Compared to TNAs (curve a of Fig. 3C), a typically anodic photocurrent for TNA/QD could be observed under visible light irradiation at an applied potential of +0.2 V (curve b of Fig. 3C). However, when the TNA/QD was immersed in a 10 mM Tris-HCl buffer solution (pH 8.0) containing iron (III), the photocurrent decreased gradually (curve c-g of Fig. 3C). After addition of ATP, the photocurrent would recovery (curve a-f of Fig. 3D). Further adding ALP enzyme, the photocurrent decreased again (curve g of Fig. 3D). It was because that, the band gap of CdTe QDs prepared for 90 min was calculated to be 2.26 eV from the UV-vis absorption spectra (Fig. 1B), and the CB and VB positions of CdTe QDs was -3.61 eV and -5.87 eV, respectively according to the formal redox potential with -1.03 V (vs. SCE, Fig. 3E). The CB of TNA at -4.21 eV was more positive than that of CdTe QDs [26], the photo-excited electrons could quickly transfer from the CB of CdTe QDs to that of TNAs, resulting in the photocurrent improvement of TNAs. However, after adding iron (III), it could chelate with CdTe QDs by amino and carboxyl groups, making the photo-excited electron from the CB of CdTe QDs (i.e., donor) to the unfilled *d* shell of iron (III), not to that of TNAs, due to the reduction potential of iron (III) and CdTe QDs of +0.05 V and-1.29 V (vs. SCE, Fig. 3 E and F) respectively, leading to the photocurrent decrease of TNA/QD. Further adding ATP, iron (III) could coordinate with ATP through triphosphate group, weaken the interaction between iron (III) and CdTe QDs, leading to the recovery of TNA/QD photocurrent. If ALP enzyme was added into the above solution, ATP would be dephosphorylated to adenosine catalyzed by ALP, which was difficult to combine with iron (III). Therefore, iron (III) would recombine with CdTe QDs, leading to the decrease of TNA/QD photocurrent again.

*3.3. Optimization of experimental conditions on the TNA/QD biosensor*

In the present work, the added amount of iron (III) or ATP had significant effect on the photocurrent response of the TNA/QD biosensor. The results showed that, with the increase of iron (III) concentration, the photocurrent of TNA/QD gradually decreased. When the concentration of iron (III) was 0.4 μM, the photocurrent tends to be stable (Fig. 4A). When ATP was added in the solution, the photocurrent recovered, and the recovery value reached to a maximum at the concentration of ATP with 0.5 μM (Fig. 4B). So, 0.4 μM of iron (III) and 0.5 μM of ATP were used in the subsequent experiments.

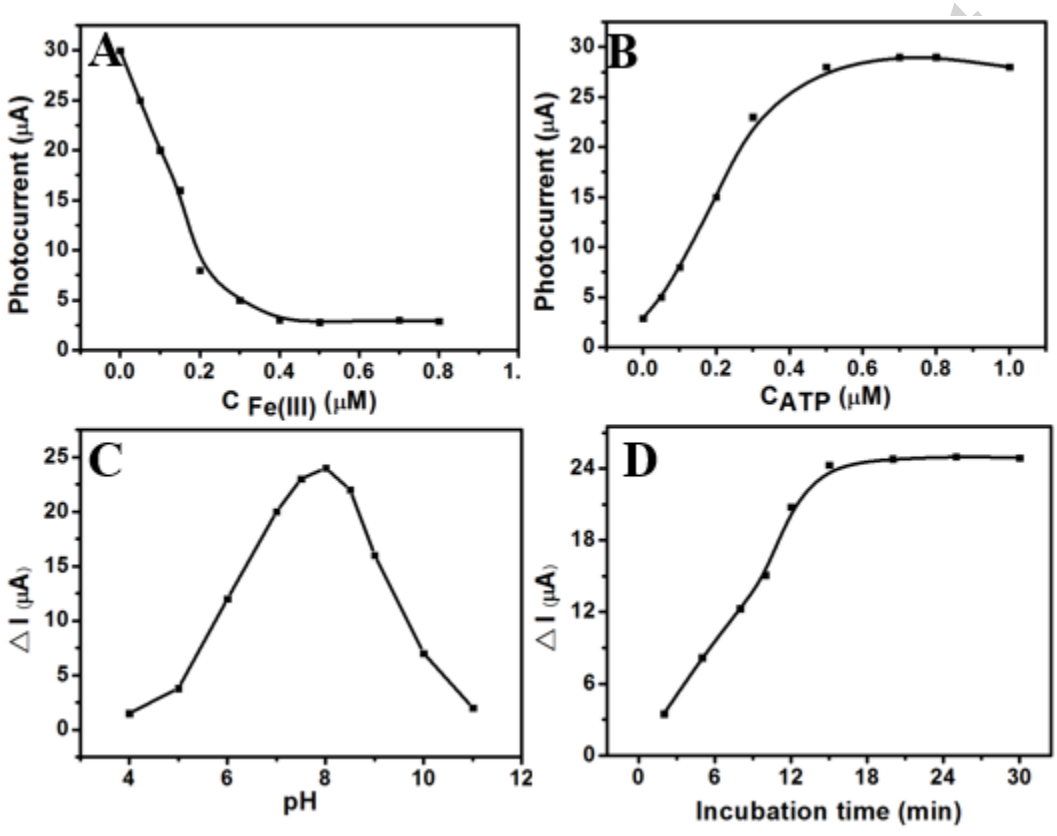


**Fig. 4.** Effect of experimental conditions on the photocurrent response of TNA/QD PEC biosensor. (A) Effect of iron (III) concentration (0-0.8 μM). (B) Effect of ATP concentration (0-1.0 μM). (C) Effect of pH from 4.0 to 10.0. (D) Effect of incubation time from 4 to 30 min.

In addition, the medium pH affects both the enzyme activity and the state of iron (III) in solution. The photocurrent response was measured in the range of pH 4.0-11.0 in 10 mM Tris-HCl buffer solution. The results showed that (Fig. 4C), the photocurrent response increased at first with

increasing pH of solution, the maximum response was obtained at pH 8.0. But the photocurrent decreased when the pH was larger than 8.0. It was because that, the catalytic activity of ALP enzyme would be inhibited in too acidic solution, and iron (III) would be hydrolyzed to form $Fe(OH)_3$ in too alkaline solution, affecting its combination with CdTe QDs or ATP. So, 10 mM Tris-HCl buffer solution with pH 8.0 was used in the experiments, which not only ensured the high catalytic activity of ALP enzyme, but also ensured the steady state of iron (III). Furthermore, the influence of the incubation time after addition of ALP on the response of the TNA/QD PEC biosensor was investigated (Fig. 4D). The photocurrent leveled off after 15 min, indicating that the catalytic reaction attained the maximum. Thus, 20 min was selected as the incubation time for the PEC biosensor.

*3.4. Determination of ALP activity and effect of inhibitor*

Under the optimized experimental conditions, different concentrations of ALP were tested by the present biosensor. Fig. 5A showed that the photocurrent of the TNA/QD biosensor decreased with the increase of ALP concentration, and the change value of photocurrent was linear with the ALP concentration in the range of 0.2 to 15 U $L^{-1}$ (Fig. 5B), the linear fitting equation was $\triangle I = 1.6775C\ (U\ L^{-1}) + 0.6028$ ($R^2 = 0.9914$), the limit of detection (LOD) of such biosensor was 0.05 U $L^{-1}$ (S/N=3), and the limits of quantification (LOQs) (S/N=10) was 0.15 U $L^{-1}$, which indicated the TNA/QD could be applied for the evaluation of ALP activity in human body because the normal ALP levels in adult serums are approximately 20 to 160 U $L^{-1}$ [3]. Compared to other methods in Table 1, the proposed assay for ALP determination exhibited an ideal measurement range and high sensitivity.

The reproducibility and selectivity of the TNA/QD PEC biosensor were investigated. For the

single TNA/QD biosensor, the relative standard deviation (RSD) was evaluated to be 2.5% for 12 successive measurements. And the RSD was calculated to be 6.8% for 5 biosensors, which indicated good reproducibility of the biosensor. To study the selectivity of the biosensor, other nonspecific proteins including protein kinase A (PKA), glucose oxidase (GOD), horseradish peroxidase (HRP), alcohol dehydrogenase (ADH), and human serum albumin (HSA) were introduced as control. The result showed that (Fig 5C), the TNA/QD biosensor had almost no response to these interfering proteins, even if their concentration were 20 times that of ALP, which indicated the proposed method has high selectivity toward ALP determination. In addition, common interfering cations in real samples, such as $Na^{+}$, $K^{+}$, $Ca^{2+}$, $Mg^{2+}$, $Zn^{2+}$, $Mn^{2+}$ and $Fe^{2+}$ with the concentration of 1.0 mM, had also little effect on the analytical results.

**Table 1** Comparison of the proposed method for ALP determination with other previously reported works.

| Methods | Linear range (U $L^{-1}$) | LOD (U $L^{-1}$) | Reference |
|---|---|---|---|
| Electrochemical | 0.1-5 | 0.03 | 10 |
| PEC | 0.5-40 | 0.33 | 15 |
| PEC | 0.003-1 | 0.001 | 16 |
| FRET | 30-1650 | 8.45 | 38 |
| Electrochemical | 1-500 | 0.5 | 39 |
| Fluorescence turn-on approach | 0-8 | 0.1 | 40 |
| Colorimetric and SERS dual-readout | 0.5-10 | 0.1 | 41 |
| Colorimetric | 0.07-300 | 0.07 | 42 |
| Fluorescence quenching | 2.5-40 | 1 | 43 |
| Real-time ratiometric fluorescent | 25-200 | 10 | 44 |
| Label-free fluorescence | 50-1000 | 10 | 45 |
| PET-based PEC | 0.2-15 | 0.05 | This work |

Furthermore, $Na_3VO_4$, a common ALP inhibitor, was introduced into the iron-ATP-ALP system to evaluate the efficiency of ALP inhibitor. The results showed that (Fig. 5D), the

photocurrent recovered gradually with the increase of $Na_3VO_4$ concentration. The $IC_{50}$ value of $Na_3VO_4$ was estimated to be 2.54 μM, which suggested that the proposed biosensor could be used for potential ALP inhibitor screening in drug discovery.

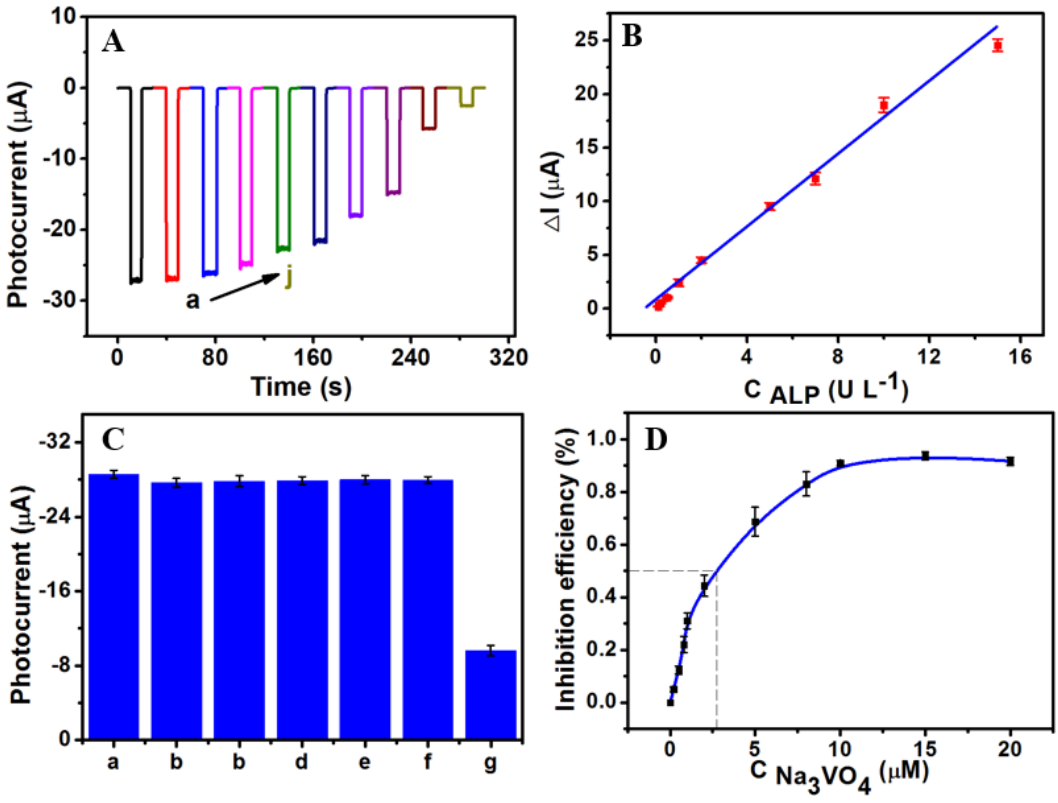


**Fig. 5.** (A) Photocurrent responses of TNA/QD biosensor under visible light irradiation after immersing in 10 mM pH 8.0 Tris-HCl buffer solution containing 0.4 μM of Fe(III), 0.5 μM of ATP and ALP with 0 (a), 0.1 (b), 0.2 (c), 0.5 (d), 1.0 (e), 2.0 (f), 5.0 (g), 7.0 (h), 10 (i) and 15 U $L^{-1}$ (j), respectively. (B) Calibration curve of photocurrent response change of the biosensor versus ALP concentration in the ranges of 0.2-15.0 U $L^{-1}$, applied potential, +0.2 V. (C) Photocurrent change of the PEC biosensor after immersing in 10 mM pH 8.0 Tris-HCl buffer solution containing 0.4 μM of Fe(III), 0.5 μM of ATP (a) and 200 U $L^{-1}$ of PKA (b), GOD (c), HRP (d), ADH (e), HSA (f), or 10 U $L^{-1}$ of ALP (h). (D) Plot of the inhibition efficiency versus $Na_3VO_4$ concentration.

*3.5. Application*

To evaluate analytical reliability and application potential of the proposed TNA/QD PEC biosensor, the ALP activity was determined in 1% (v/v) human serum and the spiked experiment was carried out when 0.5 U $L^{-1}$, 2.0 U $L^{-1}$ or 5.0 U $L^{-1}$ of ALP was added into 1% (v/v) human

serum, respectively. As seen in Table 2, the RSD values of the analytical results were between 2.8% and 5.4%, and the recoveries for the spiked samples ranged from 91% to 112%, which implied the PEC biosensor had a good accuracy and could be applied for practical analysis. In addition, the proposed PEC biosensor could be regenerated simply for repeated use by immersing in the iron (III) and ATP mixing solution according to experimental section, which could maintain ~90% activity upon repetition of these regeneration steps for 20 cycles, showing an excellent reusability. Furthermore, compared to others PEC methods for ALP determination [15,16], the proposed method was simple and time-saving, the entire analysis process took a relatively short time and lasted about 1.0 h for each sample including detection and regeneration steps.

**Table 2** Determination of ALP activity with the proposed PEC biosensor.

| Sample | Spiked (U $L^{-1}$) | Found (U $L^{-1}$) | Recovery (%) | RSD (%, n=6) |
|---|---|---|---|---|
| human serum | 0.50 | 0.56 | 112 | 5.4 |
| | 2.00 | 1.82 | 91 | 3.2 |
| | 5.00 | 5.12 | 102 | 2.8 |

## Conclusions

In summary, CdTe QDs immobilized on the TNAs improved the photocurrent response of TNAs under visible light irradiation. Addition of iron (III), followed by the addition of ATP could effectively adjust the photocurrent of TNAs due to the photo-excited electron transfer from CdTe QDs to iron (III) and the reaction of iron (III) and ATP, indicating the feasibility for determination of ALP activity based on its catalysis toward dephosphorylation of ATP. Under the optimal experimental conditions, the constructed TNA/QD PEC biosensor exhibited a satisfactory quantitative determination for the of ALP activity with high selectivity, good precision, and high

accuracy, which has been successfully applied for the ALP analysis in the real human serum, and can be expected to have potential applications for the other biomolecule analysis.

## Acknowledgements

We gratefully appreciate the financial support from the Top-notch Academic Programs Project of Jiangsu Higher Education Institutions (TAPP), the Science and Technology Project of Xuzhou City (KH17027), the Undergraduate Students Project of Jiangsu Province (201810320032Z), and the Natural Science Foundation of Jiangsu Normal University (15XLR007).

## References

[1] M.C.L. Yeung, V.W.W. Yam, Phosphate derivative-induced supramolecular assembly and NIR-emissive behavior of alkynylplatinum (II) terpyridine complexes for real-time monitoring of enzymatic activities, Chem. Sci. 4 (2013) 2928-2935.

[2] J.E. Coleman, Structure and mechanism of alkaline phosphatase, Annu. Rev. Biophys. Biomol. Struct. 21 (1992) 441-483.

[3] H.M. Wang, L.X. Mu, G.W. She, H.T. Xu, W.S. Shi, Fluorescent biosensor for alkaline phosphatase based on fluorescein derivatives modified silicon nanowires, Sens. Actuators B Chem. 203 (2014) 774-781.

[4] S. Goggins, C. Naz, B.J. Marsh, C.G. Frost, Ratiometric electrochemical detection of alkaline phosphatase, Chem. Commun. 51 (2015) 561-564.

[5] K. Ooi, K. Shiraki, Y. Morishita, T. Nobori, High-molecular intestinal alkaline phosphatase in

chronic liver diseases, J. Clin. Lab. Anal. 21 (2007) 133-139.

[6] D.V. Makarov, S. Loeb, R.H. Getzenberg, A.W. Partin, Biomarkers for prostate cancer, Annu. Rev. Med. 60 (2009) 139-151.

[7] J.J. Deng, Q. Jiang, Y.X. Wang, L.F. Yang, P. Yu, L.Q. Mao, Real-time colorimetric assay of inorganic pyrophosphatase activity based on reversibly competitive coordination of $Cu^{2+}$ between cysteine and pyrophosphate ion, Anal. Chem. 85 (2013) 9409-9415.

[8] J.J. Yang, L. Zheng, Y. Wang, W. Li, J.L. Zhang, J.J. Gu, Y. Fu, Guanine-rich DNA-based peroxidase mimetics for colorimetric assays of alkaline phosphatase, Biosens. Bioelectron. 77 (2016) 549-556.

[9] Y. Choi, N.H. Ho, C.H. Tung, Sensing phosphatase activity by using gold nanoparticles, Angew. Chem. Int. Ed. 46 (2007) 707-709.

[10] Y.Q. Liu, E.H. Xiong, X.Y. Li, J.J. Li, X.H. Zhang, J.H. Chen, Sensitive electrochemical assay of alkaline phosphatase activity based on TdT-mediated hemin/G-quadruplex DNAzyme nanowires for signal amplification, Biosens. Bioelectron. 87 (2017) 970-975.

[11] J. Peng, X.X. Han, Q.C. Zhang, H.Q. Yao, Z.N. Gao, Copper sulfide nanoparticle-decorated graphene as a catalytic amplification platform for electrochemical detection of alkaline phosphatase activity, Anal. Chim. Acta 878 (2015) 87-94.

[12] E.K. Lim, J.O. Keem, H.S. Yun, J. Jung, B.H. Chung, Smart nanoprobes for the detection of alkaline phosphatase activity during osteoblast differentiation, Chem. Commun. 51 (2015) 3270-3272.

[13] M.I. Halawa, W.Y. Gao, M. Saqib, S.A. Kitte, F.X. Wu, G.S. Xu, Sensitive detection of alkaline phosphatase by switching on gold nanoclusters fluorescence quenched by pyridoxal

phosphate, Biosens. Bioelectron. 95 (2017) 8-14.

[14] J.Y. Li, L. Si, J.C. Bao, Z.Y. Wang, Z.H. Dai, Fluorescence regulation of poly (thymine)-templated copper nanoparticles via an enzyme-triggered reaction towards sensitive and selective detection of alkaline phosphatase, Anal. Chem. 89 (2017) 3681-3686.

[15] N. Zhang, Y.F. Ruan, L.B. Zhang, W.W. Zhao, J.J. Xu, H.Y. Chen, Nanochannels photoelectrochemical biosensor, Anal. Chem. 90 (2018) 2341-2347.

[16] Q. Kang, X.X. Wang, X.L. Ma, L.Q. Kong, P. Zhang, D.Z. Shen, Sensitive detection of ascorbic acid and alkaline phosphatase activity by double-channel photoelectrochemical detection design based on g-$C_3N_4$/$TiO_2$ nanotubes hybrid film, Sens. Actuators B Chem. 230 (2016) 231-241.

[17] W.W. Zhao, J.J. Xu, H.Y. Chen, Photoelectrochemical DNA biosensors, Chem. Rev. 114 (2014) 7421-7441.

[18] L.P. Mei, F. Liu, J.B. Pan, W.W. Zhao, J.J. Xu, H.Y. Chen, Enediol-ligands-encapsulated liposomes enables sensitive immunoassay: A proof-of-concept for general liposomes-based photoelectrochemical bioanalysis, Anal. Chem. 89 (2017) 6300-6304.

[19] L.N. Wang, W.G. Ma, S.Y. Gan, D.X. Han, Q.X. Zhang, L. Niu, Engineered photoelectrochemical platform for rational global antioxidant capacity evaluation based on ultrasensitive sulfonated graphene-$TiO_2$ nanohybrid, Anal. Chem. 86 (2014) 10171-10178.

[20] M.R. Awual, New type mesoporous conjugate material for selective optical copper (II) ions monitoring & removal from polluted waters, Chem. Eng. J. 307 (2017) 85-94.

[21] M.R. Awual, Solid phase sensitive palladium(II) ions detection and recovery using ligand based efficient conjugate nanomaterials, Chem. Eng. J. 300 (2016) 264-272.

[22] M.R. Awual, M.M. Hasa, A novel fine-tuning mesoporous adsorbent for simultaneous lead(II) detection and removal from wastewater, Sens. Actuators B Chem. 202 (2014) 395-403.

[23] M.R. Awual, M.A. Khaleque, Y. Ratna, H. Znad, Simultaneous ultra-trace palladium(II) detection and recovery from wastewater using new class meso-adsorbent, J. Ind. Eng. Chem. 21 (2015) 405-413.

[24] J. Tang, Y.C. Wang, J. Li, P.M. Da, J. Geng, G.F. Zheng, Sensitive enzymatic glucose detection by $TiO_2$ nanowire photoelectrochemical biosensors, J. Mater. Chem. A 2 (2014) 6153-6157.

[25] T. Tachikawa, N. Wang, S. Yamashita, S.C. Cui, T. Majima, Design of a highly sensitive fluorescent probe for interfacial electron transfer on a $TiO_2$ surface, Angew. Chem. Int. Ed. 49 (2010) 8593-8597.

[26] T. Tachikawa, S. Yamashita, T. Majima, Evidence for crystal-Face-dependent $TiO_2$ photocatalysis from single-molecule imaging and kinetic analysis, J. Am. Chem. Soc. 133 (2011) 7197-7204.

[27] W. Zhao, Y.L. Sun, F.N. Castellano, Visible-light induced water detoxification catalyzed by Pt-II dye sensitized titania, J. Am. Chem. Soc. 130 (2008) 12566-12567.

[28] H.Y. Wang, G.M. Wang, Y.C. Ling, M. Lepert, C.C. Wang, J.Z. Zhang, Y. Li, Photoelectrochemical study of oxygen deficient $TiO_2$ nanowire arrays with CdS quantum dot sensitization, Nanoscale 4 (2012) 1463-1466.

[29] X. Yan, X. Cui, B.S. Li, L.S. Li, Large, solution- processable graphene quantum dots as light absorbers for photovoltaics, Nano Lett. 10 (2010) 1869-1873.

[30] V. Gupta, N. Chaudhary, R. Srivastava, G.D. Sharma, R. Bhardwaj, S. Chand, Luminscent

graphene quantum dots for organic photovoltaic devices, J. Am. Chem. Soc. 133 (2011) 9960-9963.

[31] J.Y. Tian, Y. Li, J.J. Dong, M.J. Huang, J.S. Lu, Photoelectrochemical $TiO_2$ nanotube arrays biosensor for asulam determination based on in-situ generation of quantum dots, Biosens. Bioelectron. 110 (2018) 1-7.

[32] Y. Li, J.Y. Tian, T. Yuan, P. Wang, J.S. Lu, A sensitive photoelectrochemical aptasensor for oxytetracycline based on a signal "switch off-on" strategy, Sens. Actuators B Chem. 240 (2017) 785-792.

[33] J.S. Lu, H.N. Li, D.M. Cui, Y.J. Zhang, S.Q. Liu, Enhanced enzymatic reactivity for electrochemically driven drug metabolism by confining cytochrome P450 enzyme in $TiO_2$ nanotube arrays, Anal. Chem. 86 (2014) 8003-8009.

[34] A. de la Escosura, M.V. Martinez Diaz, D.M. Guldi, T. Torres, Stabilization of charge-separated states in phthalocyanine- fullerene ensembles through supramolecular donor-acceptor interactions, J. Am. Chem. Soc. 128 (2006) 4112-4118.

[35] K. Abbas, H. Znad, M.R. Awual, A ligand anchored conjugate adsorbent for effective mercury(II) detection and removal from aqueous media, Chem. Eng. J. 334 (2018) 432-443.

[36] M.R. Awual, M.M. Hasan, G.E. Eldesoky, M.A. Khaleque, M.M. Rahman, M. Naushad, Facile mercury detection and removal from aqueous media involving ligand impregnated conjugate nanomaterials, Chem. Eng. J. 290 (2016) 243-251.

[37] M.R. Awual, M.M. Hasan, T. Ihara, T. Yaita, Mesoporous silica based novel conjugate adsorbent for efficient selenium(IV) detection and removal from water, Microporous Mesoporous Mater. 196 (2014) 261-269.

[38] B.H. Li, Y.L. Zhang, F.S. Li, W. Wang, J. Liu, M. Liu, Y. Cui, X.B. Li, B.L. Li, A novel sensor for the detection of alkaline phosphatase activity based on the self-assembly of $Eu^{3+}$-doped oxide nanoparticles and heptamethine cyanine dye, Sens. Actuators B Chem. 233 (2016) 479-485.

[39] C.C. Shen, X.Z. Li, A. Rasooly, L.Y. Guo, K.N. Zhang, M.H. Yang, A single electrochemical biosensor for detecting the activity and inhibition of both protein kinase and alkaline phosphatase based on phosphate ions induced deposition of redox precipitates, Biosens. Bioelectron. 85 (2016) 220-225.

[40] H.S. Liu, C.B. Ma, J. Wang, K.M. Wang, K.F. Wu, A turn-on fluorescent method for determination of the activity of alkaline phosphatase based on dsDNA-templated copper nanoparticles and exonuclease based amplification, Microchim. Acta 184 (2017) 2483-2488.

[41] J. Zhang, L.F. He, X. Zhang, J.P. Wang, L. Yang, B.H. Liu, C.L. Jiang, Z.P. Zhang, Colorimetric and SERS dual-readout for assaying alkaline phosphatase activity by ascorbic acid induced aggregation of Ag coated Au nanoparticles, Sens. Actuators B Chem. 253 (2017) 839-845.

[42] Z.W. Tang, H.F. Zhang, C.B. Ma, P. Gu, G.H. Zhang, K.F. Wu, M.J. Chen, K.M. Wang, Colorimetric determination of the activity of alkaline phosphatase based on the use of Cu(II)-modulated G-quadruplex-based DNAzymes, Microchim. Acta 185 (2018) 109-115.

[43] Y.Q. Mei, Q. Hu, B.J. Zhou, Y.H. Zhang, M.H. He, T. Xu, F. Li, J.M. Kong, Fluorescence quenching based alkaline phosphatase activity detection, Talanta 176 (2018) 52-58.

[44] J.J. Deng, P. Yu, Y.X. Wang, L.Q. Mao, Real-time ratiometric fluorescent assay for alkaline phosphatase activity with stimulus responsive infinite coordination polymer nanoparticles,

Anal. Chem. 87 (2015) 3080-3086.

[45] Y.N. Li, Y. Li, X.Y. Wang, X.G. Su, A label-free conjugated polymer-based fluorescence assay for the determination of adenosine triphosphate and alkaline phosphatase, New J. Chem. 38 (2014) 4574-4579.

## Graphical Abstract

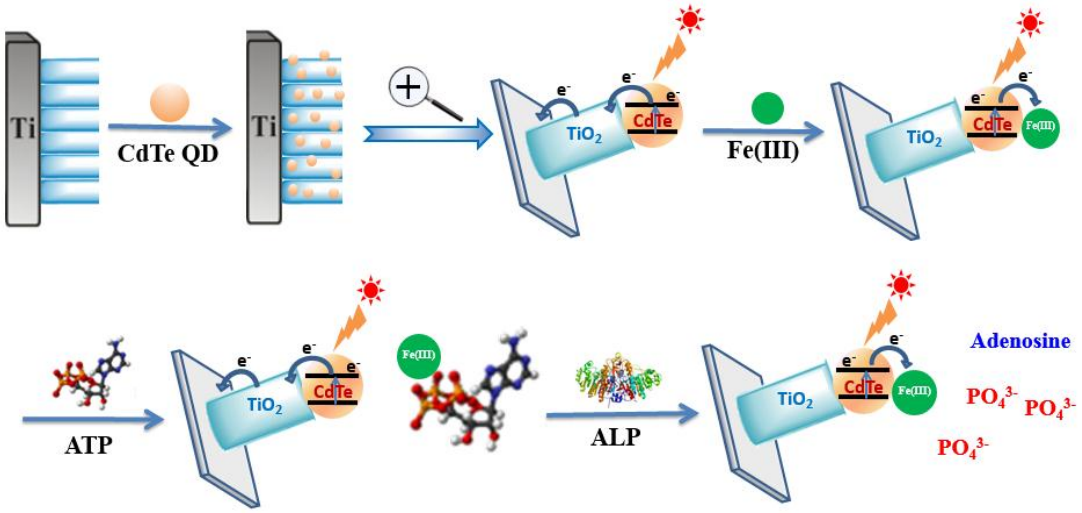


## Highlights

- A sensitive PEC biosensor for ALP activity based on photo-excited electron transfer.
- Controllable electron transfer adjustment among TNAs, CdTe QDs and iron (III) by ALP catalysis.
- Determination of ALP activity with wider linear range of 0.2-15 U $L^{-1}$ and lower LOD of 0.05 U $L^{-1}$.
- Analysis of real samples with good accuracy, selectivity, reproducibility and stability.